Towards 3D Reconstruction of Endoscope Images Using Shape from Shading

CARLOS HENRIQUE QUARTUCCI FORSTER
CLÉSIO L. TOZZI
Dept. of Computer Engineering and Industrial Automation - DCA
School of Electrical and Computer Engineering - FEEC
State University of Campinas - UNICAMP
C.P. 6101, 13083-970 - Campinas, SP, Brazil

{forster,clesio}@dca.fee.unicamp.br

Abstract – The 3D Reconstruction problem from a single endoscope image of a smooth object is studied in the context of the Shape from Shading methods and considering a single light source at the camera projection center. Based on a curve expansion Shape from Shading algorithm, a spherical projection model for the endoscope camera and a dichromatic model for the surface reflectance, an approach to solve practical problems, namely the endoscope image distortion and the removal of the image specular reflection component, is presented. Results obtained from application of this approach to synthetic and real images are presented.

Keywords – Color image, dichromatic model, endoscope imaging, image distortion, shape from shading.

1 Introduction

Geometrical data reconstruction from images is an important problem in Computer Vision. The recovered geometry information can be used to manipulate and visualize the real object in a virtual environment. For medical applications, such as endoscope imagery, 3D reconstruction can be used to produce better visualization, improve measurement or study, for example, the evolution of tumors. The common endoscope is based on a single camera and one single light source, suggesting the use of the Shape from Shading (SFS) technique as the most convenient approach to 3D reconstruction of surfaces imaged using this equipment.

The SFS problem consists of the solution of the image irradiance equation as introduced by Horn [1975]. The three main approaches proposed in the literature to solve the SFS problem are based on optimization, curve expansion and local analysis. These approaches are discussed, for example, in [Pentland 1984], [Lee and Rosenfeld 1985], [Zheng and Chellappa 1991] and [Šára 1995] for local analysis methods, [Zheng and Chellappa 1991], [Horn 1990], [Ikeuchi and Horn 1981], [Szeliski 1991] and [Lai and Vemuri 1997] for optimization based methods and [Kimmel and Bruckstein 1995a] and [Horn 1975] for curve expansion based methods.

Okatani and Deguchi [1997] based on the fact that the light source is very close to the camera on the endoscope head, assumed the endoscope imaging model to be composed by a light source at the projection center and proposed an approach based on curve expansion for the reconstruction of endoscope images.

There are some important conditions found in practice that are not considered in the Okatani-Deguchi [1997] model. One such condition follows from the fact that the endoscope camera must be very close to the object of interest, demanding small focal distance lenses (wide-angle or fisheye lenses) that results in a strong radial image distortion. Other problem relevant to endoscope image reconstruction by SFS is the usual assumption of a Lambertian surface, that may result in errors since surfaces often considered in endoscope images do not present the Lambertian reflectance characteristic.

Considering these conditions, this paper proposes to include in Okatani-Deguchi [1997] model a solution to them. A spherical projection model is assumed to model the camera. The image distortion parameter, determined using a set of calibration images, is included in the SFS solution. Concerning the Lambertian surface assumption, a dichromatic model is used to remove the specular reflection component present in the image, in order to obtain a Lambertian surface equivalent image.

The paper is organized as follows: in Section 2 the Shape from Shading problem solution based on curve expansion is reviewed; in Section 3 the dichromatic model and the removal of the specular component from the image is presented; in Section 4 the endoscope camera model is presented and discussed; in Section 5, the adjustment of Okatani and Deguchi [1997] model for the proposed approach is considered; in Section 6 the results obtained from the application of this approach to real and synthetic images are presented and, finally, the conclusions are presented in Section 7.

0-7695-0878-2/00 $10.00 © 2000 IEEE

2 The Shape from Shading Algorithm

The Okatani and Deguchi [1997] algorithm, that will be used for the implementation proposed in this paper, is an adjustment of the Kimmel and Bruckstein [1995a] algorithm and supposes that an initial curve of constant depth is known (initial guess) and the remaining constant depth curves, covering all the image plane, are determined by the expansion of the initial curve.

The curve expansion process is described by a time-based differential equation system in which the depth variable is proportional to time. According to Kimmel and Bruckstein [1995a], in the case of a Lambertian surface, orthographic projection and light source direction perpendicular to the image plane, for a constant depth curve represented in the parametric form $C(z) = \{\forall s, (x(s), y(s))\}$, the expansion equations can be written as

$$\begin{cases} x_t(s,z) = \dfrac{y_s}{\sqrt{x_s^2 + y_s^2}} \dfrac{E}{\sqrt{1-E^2}} \\ y_t(s,z) = \dfrac{-x_s}{\sqrt{x_s^2 + y_s^2}} \dfrac{E}{\sqrt{1-E^2}} \end{cases} \quad (1)$$

where $E(x,y)$ is the image intensity or irradiance and the variable subscript represents the partial derivative.

The curve expansion equation system (1) can be rewritten as

$$C_t = F \cdot \hat{n} \quad (2)$$

where $\hat{n}$ is the curve normal vector and F is the curve normal speed given by

$$F = \frac{E}{\sqrt{1-E^2}} \quad (3).$$

Numerical instability and topological problems can be observed in this formulation unless a rediscretization scheme is applied to the expanding curve at each iteration. To overcome the numerical instability and topological problems arising from the solution of an equation system such as the one described by equations (1), Kimmel and Bruckstein [1995a] employed the numerical method presented by Osher and Sethian [1988] in which the expanding curve is represented by an implicit function.

For this numerical method, the function $\phi(x,y,t)$ represents a curve for which $\phi(x,y,t) = 0$ in the points (x,y) belonging to the curve of constant depth $C(t)$. The objective is the expansion of an initial curve represented by $\phi(x,y,0) = 0$ in a way that $\phi(x,y,t) = 0$ represents the curve $C(t)$ at any time t. If the light source direction is taken parallel to the z axis, the expansion equation is represented by

$$\phi_t = F(x,y)\sqrt{\phi_x^2 + \phi_y^2} \quad (4).$$

The numerical method solution for curve expansion is implemented by an iterative algorithm. Initially the iteration index variable n, for which $t = n \cdot \Delta t$, is made equal to zero and the initial function ϕ^n (equation 4) is evolved in order to obtain ϕ^{n+1}. For the pixels where $\phi^n \cdot \phi^{n+1} < 0$, the time value corresponding to the index variable n is assigned to the pixel depth variable. In the sequence, n is incremented and the above procedure is repeated until depth values have been assigned to all the pixels in the image.

In order to solve equation (4) an initial function must be provided. A conic function centered in a singular point can be considered as initial function. Another usual approach is the application of a threshold to the intensity image to obtain this initial function.

For this algorithm, depending on the configuration of singular points, the obtained solution is strongly influenced by the selected singular point. Knowing singular point depths or the surface topology, a global solution can be obtained by merging local solutions obtained for each singular point. Kimmel and Bruckstein [1995b] and Shimshoni *et al.* [1996] propose an extension to the Kimmel and Bruckstein [1995a] algorithm in order to obtain a global solution. Also, an approach for a global solution for the case of many singular points whose depths are known is found in Oliensis and Dupuis [1994].

For the endoscope case Okatani and Deguchi [1997], based on Kimmel and Bruckstein [1995a] and considering the light source and the camera projection center at the same position and near to the surface, modeled the endoscope image formation process through the equation

$$E(x,y) = \rho \frac{G(\cos\theta)}{r^2} \quad (5)$$

where $E(x,y)$ is the image intensity or irradiance, ρ is the surface albedo, θ is the angle between the surface normal and the observer direction (coincident with the light source direction in this case), r is the distance between the projection center and the corresponding point on the surface and the function $G(\cos\theta)$ is considered to adjust the reflectance map for the case of a non-Lambertian surface.

Differently from [Kimmel and Bruckstein 1995a], where the z coordinate representation is considered, Okatani and Deguchi [1997] represented the constant depth curves by the distance from the surface point to the projection center, expressed by the equation

$$r(x,y) = \sqrt{x^2 + y^2 + z^2}.$$

Given this representation for the constant depth curves, the equation (4) was rewritten by Okatani and Deguchi [1997] resulting in

$$\phi_t = -\frac{G^{-1}\left(t^2 E(x,y)/\rho\right)}{z_{pi}\, t\sqrt{1-\left(G^{-1}\left(t^2 E(x,y)/\rho\right)\right)^2}} \cdot \frac{}{\sqrt{\left(x^2+y^2+z_{pi}^{\ 2}\right)\left(\left(x^2+z_{pi}^{\ 2}\right)\phi_x^{\ 2}+2xy\phi_x\phi_y+\left(y^2+z_{pi}^{\ 2}\right)\phi_y^{\ 2}\right)}} \quad (6)$$

where z_{pi} is the focal length.

3 Removal of Specular Reflection

The dichromatic model as described by [Tominaga 1991], [Tominaga 1998] and [Tian and Tsui 1997] is based on the fact that some surfaces can be modeled by the superposition of two layers: one composed of the true surface material, namely the body layer, whose reflectance is assumed Lambertian, and the other, made of materials such as resin, wax or oil, forming the interface layer between the body layer and the atmosphere, being the latter determinant of the specular reflection. Intuitively, the reflection due to the body layer and the interface layer can be considered dependent on the body material color and the light color, respectively. Letting λ be the wavelength or the index to a base function defined over the wavelength domain, $E(\lambda)$ the incident light intensity, $S_I(\lambda)$ the reflectance due to the interface layer, $S_B(\lambda)$ the reflectance of the body layer and θ the variable describing all the geometric dependencies of the scene, the reflected light intensity $Y(\theta,\lambda)$ is given by the equation

$$Y(\theta,\lambda) = c_I(\theta)S_I(\lambda)E(\lambda) + c_B(\theta)S_B(\lambda)E(\lambda) \quad (7)$$

where $c_I(\theta)$ and $c_B(\theta)$ are constants dependent on the reflectance maps of the interface and the surface body layer, respectively.

According to Tominaga [1991], who employed the dichromatic model for object identification, plastic, paints, china, vinyl, tile, fruit, leaves and woods can be described by this model, while materials such as papers, metal and cloth do not comply with the model.

As observed in Section 1, usually the SFS algorithm assumes the surface reflectance to be Lambertian. An equivalent Lambertian surface image can be obtained from the image of a surface that by hypothesis fulfills the dichromatic reflection model characteristics using the procedure presented in the sequence.

Let $[I_r, I_g, I_b]^T$ be the vector representing the three color components of a pixel R, G and B, $[kd_r, kd_g, kd_b]^T$ be the vector representing the body reflection coefficients and $[ks_r, ks_g, ks_b]^T$ the vector representing the interface reflection coefficients. For white light, $E = [1,1,1]^T$. If the body reflection is assumed to be Lambertian, then $c_B(\theta) = \cos\sigma$, where σ is the angle between the light source direction and the surface normal.

From the dichromatic model,

$$Y = \begin{bmatrix} I_r \\ I_g \\ I_b \end{bmatrix} = \begin{bmatrix} kd_r & ks_r \\ kd_g & ks_g \\ kd_b & ks_b \end{bmatrix} \begin{bmatrix} c_B \\ c_I \end{bmatrix} \quad (8).$$

It is possible to choose a vector $[a_1, a_2, a_3]^T$ perpendicular to $[ks_r, ks_g, ks_b]^T$, so that

$$a_1 ks_r + a_2 ks_g + a_3 ks_b = 0 \quad (9).$$

Multiplying the lines of equation (8) by the components of $[a_1, a_2, a_3]^T$ results

$$\begin{bmatrix} a_1 I_r \\ a_2 I_g \\ a_3 I_b \end{bmatrix} = \begin{bmatrix} a_1 kd_r & a_1 ks_r \\ a_2 kd_g & a_2 ks_g \\ a_3 kd_b & a_3 ks_b \end{bmatrix} \begin{bmatrix} c_B \\ c_I \end{bmatrix} \quad (10).$$

From equation (10)

$$a_1 I_r + a_2 I_g + a_3 I_b = (a_1 kd_r + a_2 kd_g + a_3 kd_b)c_B + (a_1 ks_r + a_2 ks_g + a_3 ks_b)c_I$$

and replacing the last term by equation (9)

$$a_1 I_r + a_2 I_g + a_3 I_b = (a_1 kd_r + a_2 kd_g + a_3 kd_b)c_B .$$

It is observed from the last equation that given the vector $[a_1, a_2, a_3]^T$ perpendicular to $[ks_r, ks_g, ks_b]^T$, the coefficient $c_B(\theta)$ is proportional to $a_1 I_r + a_2 I_g + a_3 I_b$. The knowledge of $[kd_r, kd_g, kd_b]^T$ results in the exact determination of $c_B(\theta)$. However, it is difficult to find this vector in the present context and an appropriate choice for $[a_1, a_2, a_3]^T$ among those perpendicular vectors to $[ks_r, ks_g, ks_b]^T$ must be made.

Considering $[ks_r, ks_g, ks_b] = [1 \ 1 \ 1]$, i.e., the interface reflection color is the same of the light source, $[a_1, a_2, a_3] = [1 \ -1 \ 0]$ can be used. Therefore, an equivalent Lambertian reflection image can be obtained from the original image by the difference $I_r - I_g$ or any other linear combination for which $a_1 + a_2 + a_3 = 0$.

4 Radial distortion correction

In order to correct the image distortion a model based on a spherical projection followed by an orthographic projection is considered. As shown in *figure 1*, an image point (I'') is obtained by projecting a 3D space point (I) on a spherical

surface of radius f with origin at the image projection center (O) and then projecting the obtained point on the spherical surface (I') onto the image plane considering the parallel projection model. This model maps the 3D space into a circle with radius f whose boundary corresponds to the 180° field of vision.

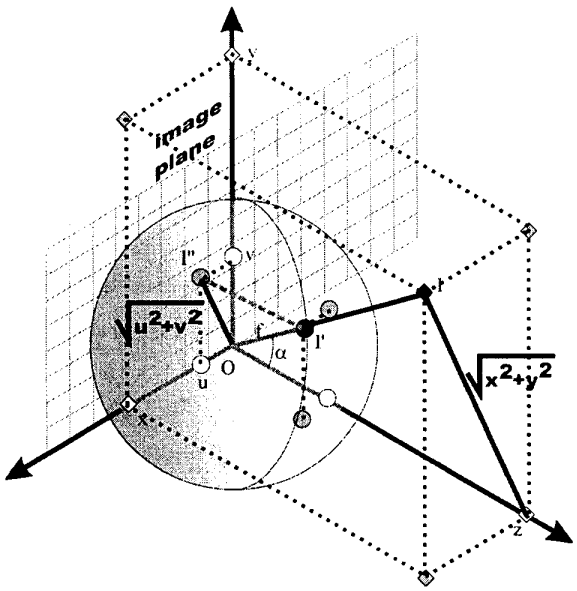

Figure 1 – The camera spherical projection model.

Let (u,v) be the coordinates in the distorted image, (x,y,z) the point coordinates measured in the 3D space coordinate system with origin at the projection center and the z axis coincident with the camera optical axis, and r the distance between the projection center and the point (x,y,z). From the triangles in *figure 1*, the following relations can be obtained:

$$r(u,v) = \sqrt{x(u,v)^2 + y(u,v)^2 + z(u,v)^2} \tag{11}$$

$$z(u,v) = \frac{\sqrt{f^2 - u^2 - v^2}}{f} r(u,v) \tag{12}$$

$$\begin{cases} x(u,v) = \dfrac{z(u,v)\cdot u}{\sqrt{f^2 - u^2 - v^2}} \\ y(u,v) = \dfrac{z(u,v)\cdot v}{\sqrt{f^2 - u^2 - v^2}} \end{cases} \tag{13}.$$

It can be observed from the equations (11) to (13), that any of the variables $z(u,v)$, $r(u,v)$, $x(u,v)$ or $y(u,v)$ carries all the depth information and one can be derived from the others. Therefore, the reconstruction solution can be expressed in any of these variables.

Given the $x(u,v)$ and $y(u,v)$ variables from the spherical projection, a warping transformation can be used to map these variables to equivalent perspective images. The warping equations can be determined applying the spherical projection model to a planar object parallel to the image plane (depth z constant and equal to the focal distance (z_{pi}) for the perspective projection).

$$x = \frac{z_{pi}\cdot u}{\sqrt{f^2 - u^2 - v^2}}\,;\, y = \frac{z_{pi}\cdot v}{\sqrt{f^2 - u^2 - v^2}}. \tag{14}$$

The warping inverse transformation is

$$u = \frac{f\cdot x}{\sqrt{z_{pi}^{\ 2} + x^2 + y^2}}\,;\, v = \frac{f\cdot y}{\sqrt{z_{pi}^{\ 2} + x^2 + y^2}}. \tag{15}$$

5 Including Camera Distortion Parameters in Okatani and Deguchi Model

In the context of this paper, the specular reflection component, as discussed in Section 3, is removed from the image by using the dichromatic model and the assumption of a Lambertian surface can be considered for the SFS problem solution. For the condition of a Lambertian surface, the function $G(\cos\theta)$ in equation (5) is reduced to $\cos\theta$.

To include the camera distortion parameter into the solution presented in equation (6) the derivatives of the implicit function ϕ described in Section 2 and computed for the perspective image must be rewritten for the case of spherical projection model adopted for the endoscope camera or the distorted coordinates converted to the perspective model.

The transformation from the distorted image to the equivalent perspective image is given by

$$\nabla\phi = \begin{bmatrix} \dfrac{\partial u}{\partial x} & \dfrac{\partial v}{\partial x} \\ \dfrac{\partial u}{\partial y} & \dfrac{\partial v}{\partial y} \end{bmatrix} \cdot \begin{bmatrix} \phi_u \\ \phi_v \end{bmatrix} \tag{16}$$

where the 2 x 2 matrix in equation (16) is the jacobian matrix for the warping equations (15).

Equation (16) can be written in expanded form as

$$\begin{aligned} \phi_x &= u_x\phi_u + v_x\phi_v \\ \phi_y &= u_y\phi_u + v_y\phi_v \end{aligned} \tag{17}.$$

The derivatives in equation (17) are given by

$$u_x = \frac{f}{\sqrt{z_{pi}^2 + x^2 + y^2}} - x^2 f \cdot (z_{pi}^2 + x^2 + y^2)^{-\frac{3}{2}},$$

$$u_y = v_x = -xyf \cdot (z_{pi}^2 + x^2 + y^2)^{-\frac{3}{2}}, \quad (18)$$

$$v_y = \frac{f}{\sqrt{z_{pi}^2 + x^2 + y^2}} - y^2 f \cdot (z_{pi}^2 + x^2 + y^2)^{-\frac{3}{2}},$$

where f is the distortion parameter (radius of the spherical projection surface).

The curve expansion equation under these conditions and considering $z_{pi} = 1$ (scale factor) and $\rho = 1$ (normalized intensity image) is given by

$$\phi_t = \frac{-tE(u,v)}{\sqrt{1-t^4E^2}} \cdot \frac{}{\sqrt{(x^2+y^2+1)\left[(x^2+1)\phi_x^2 + 2xy\phi_x\phi_y + (y^2+1)\phi_y^2\right]}}.$$

6 Results

In order to verify the applicability of this approach to the reconstruction of endoscope images, tests were made using real and synthetic images. Initially, for real images, the camera distortion parameter is determined using two alternative calibration procedures.

The first calibration procedure was conducted by printing on paper an image composed by concentric circumferences and positioning the endoscope head perpendicularly to the paper at a distance h above the center of the circumferences (see *figure 2*). In this procedure, each circumference corresponds to a value of α determined by the relation $\alpha = \tan^{-1}(r/h)$.

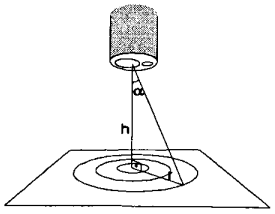

Figure 2 – Arrangement for camera calibration.

A circumference with radius $r = h$ corresponds to a 45° angle (α). Knowing the values for (u,v) from the image and the corresponding α, the distortion parameter f is determined by the equation

$$\sqrt{u^2 + v^2} = f \cdot \operatorname{sen}\alpha \quad (19)$$

derived from the analysis of the triangles in *figure 1*.

A good estimation for f can be obtained using the estimator

$$\bar{f} = \frac{1}{n}\sum_{i=1}^{n} \frac{\sqrt{u_i^2 + v_i^2}}{\operatorname{sen}\alpha_i}, \quad (20)$$

for many experimental values for the tuple (u_i, v_i, α_i).

Another approach to calibration, better than the former for the context where the correct positioning of the endoscope is not possible, can be conducted by printing a regular square grid on paper, acquiring its corresponding endoscope image and applying to the captured image the warping transformation (equations 15) considering multiple values of f. The camera distortion parameter is assigned according to the value f considered in the transformed image that by visual judgement presents the straightest lines. See example in *figure 3*.

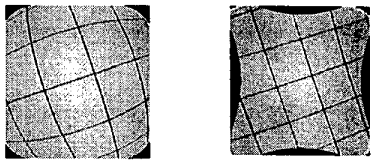

Figure 3- Result of the calibration using warping transformation (a) Original distorted image. (b) Best corrected image.

To verify the applicability of the dichromatic model for specular reflection removal, tests were made in real and synthetic images. In *figure 4* results of the specular reflection removal algorithm are presented for a synthetic ray traced image, an endoscope image and the scanned image of a resin object. The black regions around the specular points in these

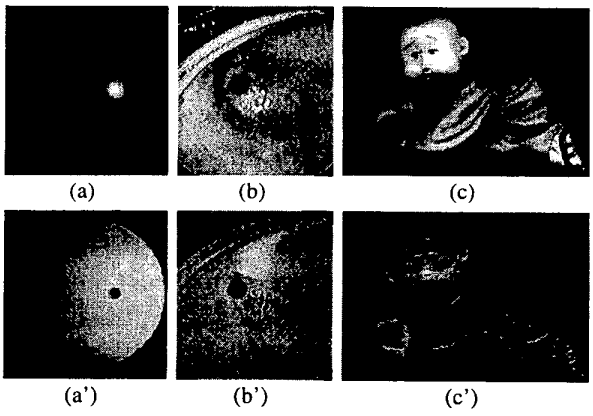

Figure 4 – Specular reflection component removal. Original and processed images: (a) Synthetic image (b) Endoscope image. (c) Scanned image of a resin object.

images are due to intensity saturation and consist of pixels whose red, green or blue intensities are above the saturation threshold. The clear region in image (4b') corresponds to the change of albedo in the surface due to the presence of bile.

The results of a SFS reconstruction for synthetic images and a real endoscope image are presented in *figure 5* and in *figure 6*, respectively.

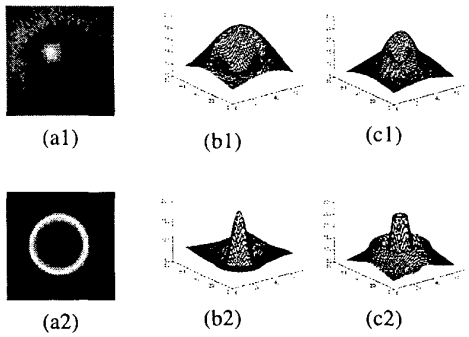

Figure 5 – Results from the SFS algorithm for synthetic images. (a) Original images (b) Original geometry. (c) Reconstructed surface using the curve expansion algorithm.

7 Conclusion

The SFS problem is often qualified as an *ill-posed* problem in the literature and its solution is considered a difficult task. Most of the approaches to solve the SFS problem result in a system of non-linear differential partial equations usually susceptible to numerical instability. The curve expansion technique employed in this paper is an alternative method to solve this kind of system of equations, demanding the determination of singular points, which can be difficult and inconvenient in many applications.

Despite the absence of a numerical error measurement evaluation, the quality of the obtained SFS reconstructed surfaces for the considered endoscope images is subjectively considered good.

Considering the removal of specular reflection in color images, the obtained results are satisfactory for synthetic images and for images of surfaces compliant with the dichromatic model. The application of the dichromatic model to surfaces usually considered for endoscope images demands further measurements and the validation of the results by endoscopy professionals.

It should be noted that endoscope images are difficult to be processed automatically. Some relevant problems include the interreflection, intensity saturation, specular reflection, non-rigid movement of digestive tract walls, difficulty to set the endoscope in the appropriate position and variability of the albedo in the digestive tract due to gastric aging, presence of blood vessels and presence of digestive liquids.

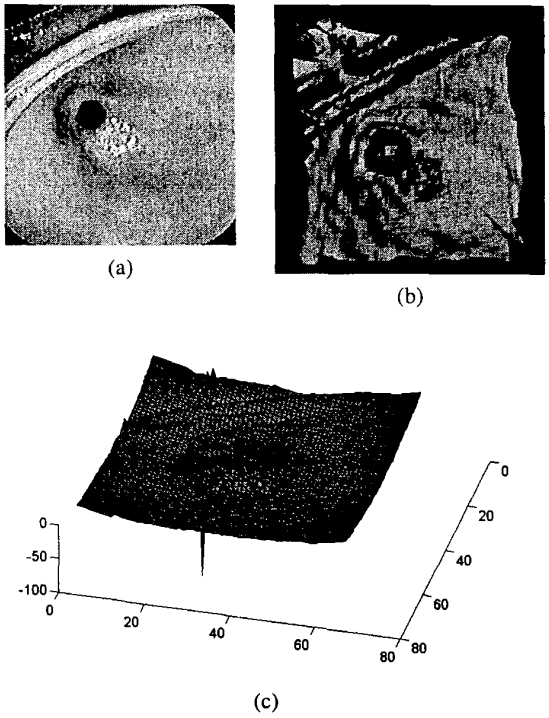

Figure 6 – Reconstruction of a real endoscope image. (a) Original endoscope image. (b) Rendered image (ray traced) for the reconstructed surface triangular mesh. (c) Depth map as function of image coordinates $z(u,v)$.

Acknowledgements

The first author (C. H. Q. F.) was supported by FAPESP (Proc. 98/04220-3).

The authors thank Dr. Fabio Guerrazzi and Dr. José Geraldo Ferraz for providing endoscope images.

References

1. Horn, B. K. P., 1975, Obtaining Shape from Shading Information, In *Shape from Shading*, pp 121-171.
2. Horn, B. K. P., 1990, *Robot Vision*, The MIT Press, Cambridge, Massachusetts.
3. Ikeuchi, K. and Horn, B. K. P., 1981, Numerical Shape from Shading and Occluding Boundaries, *Artificial Intelligence*, vol 17, no 1-3, pp 141-184.
4. Kimmel, R. and Bruckstein, A. M., 1995a, Tracking Level Sets by Level Sets: A Method for Solving the Shape from Shading Problem, *Computer Vision and Image Understanding*, vol 62, no 2, pp 47-58.
5. Kimmel, R. and Bruckstein, A. M., 1995b, Global Shape From Shading, *Computer Vision and Image Understanding*, vol 62, no 3, pp 360-369.
6. Lai, S. H. and Vemuri, B. C., 1997, Physically Based Adaptive preconditioning for Early Vision, *IEEE Transactions on Pattern Analysis and Machine Intelligence*, vol 19, no 6, pp 594-607.
7. Lee, C.and Rosenfeld A., 1985, Improved Methods of Estimating Shape from Shading Using the Light Source Coordinate System, In *Shape from Shading*.
8. Okatani, T. and Deguchi, K., 1997, Shape Reconstruction from an Endoscope Image by Shape from Shading Technique for a Point Light Source at the Projection Center, *Computer Vision and Image Understanding*, vol 66, no 2, pp 119-131.

9. Oliensis J. and Dupuis P., 1994, Shape from Shading: Provably Convergent Algorithms and Uniqueness Results, *Lecture Notes in Computer Science,* vol 801, Jan-Olof Eklundn editor, ECCV'94 vol II, Stockholm, Springer, pp 259-268.
10. Osher S. and Sethian J., 1988, Fronts Propagating with Curve-Dependent Speed: Algorithms Based on Hamilton-Jacobi Formulations, *Journal of Computational Physics,* vol 79, pp 12-49.
11. Pentland, A., 1984, Local Shading Analysis, *IEEE Transactions on Pattern Analysis and Machine Intelligence,* vol 6 no 2, pp 170-187.
12. Šára, R., 1995, Isophotes: the Key to Tractable Local Shading Analysis, *Lecture Notes in Computer Science,* vol 970, pp 416-423.
13. Shimshoni, I., Kimmel, R. and Bruckstein A. M., 1996, Global Shape from Shading, *Computer Vision and Image Understanding,* vol 64 no 1, pp 188-189.
14. Szeliski, R., 1991, Fast Shape from Shading. *CVGIP: Image Understanding,* vol 53, no 2, pp 129-153.
15. Tian, Y. and Tsui, H. T., 1997, Shape Recovery from a Color Image for Non-Lambertian Surfaces, *Journal of the optical Society of America A,* vol 14, no 2, pp 397-404.
16. Tominaga, S., 1998, Estimation of Reflection Parameters from a Color Image, *Lecture Notes in Computer Science,* vol 1351.
17. Tominaga, S., 1991, Surface Identification Using the Dichromatic Reflection Model, *IEEE Transactions on Pattern Analysis and Machine Intelligence,* vol 13, no 7, pp 658-670.
18. Zheng, Q. and Chellappa, R., 1991, Estimation of Illuminant Direction, Albedo, and Shape from Shading, *IEEE Transactions on Pattern Analysis and Machine Intelligence,* vol 13, no 7, pp 680-702.